ADVANCED FUNCTIONAL MATERIALS
www.afm-journal.de

1D Crystalline Assemblies Exhibiting Large Second Harmonic Generation Susceptibilities and Stacking-/Polarization-Driven Tunability

*Jingyu Yang, Jinbo Pan, Yan-Fang Zhang, Guolin Wan, Yongqian Zhu, Zixuan Wei, Yuhui Li, and Shixuan Du**

Nonlinear optical (NLO) van der Waals (vdW) crystals containing 1D building blocks exhibit large NLO coefficients and birefringence that are crucial for their applications. In this work, 21 NLO 1D building blocks with large second harmonic generation (SHG) susceptibility from the Computational 1D Materials Database (C1DB) are screened. Among them, 14 are hitherto unreported and have SHG susceptibilities approaching theoretical upper limits. Forty-five new vdW NLO crystals are then constructed by stacking one or two of the 21 building blocks. Eighteen of them inherit the large SHG susceptibilities of their corresponding 1D building blocks. Three stable crystals exhibit large SHG susceptibilities and birefringence, while one stable crystal possesses ferroelectricity. Interestingly, the SHG susceptibilities of the newly constructed NLO crystals are inversely proportional to the third power of their bandgaps. Further calculations show that the SHG susceptibilities of the vdW NLO crystals can be tuned either by stacking order or by reversing electric polarization, providing possibilities for their application in tunable nonlinear optics and NLO switches.

1. Introduction

The second harmonic generation (SHG) process is a coherent nonlinear process wherein two lower energy photons are upconverted to exactly twice the incident frequency (or half the wavelength) of an excitation laser.[1] This process is of great interest in photolithography, atomic clocks, communication, and so on.[2] Nonlinear optical (NLO) crystals are ideal materials that can generate SHG process. However, exploration of novel NLO crystals with large SHG susceptibilities, which is one of the key parameters of SHG,[3] remains a big challenge, especially for those used in high-power optical output.[4] Meanwhile, phase or state transitions of NLO crystals are also important for tunable NLO applications, for example, nanophotonic devices and photonic information communication.[5] Sufficiently large SHG deviations before and after transition are required for their applications.[6]

NLO crystals can be ionic crystals,[7] organic crystals,[8] or van der Waals (vdW) materials.[9] Recently, several vdW NLO crystals stacked with 1D building blocks show SHG susceptibilities approaching the theoretical upper limit across various wave ranges and large birefringence to realize phase matching.[10] Compared to high-dimensional systems, the confinement of electron motion in NLO crystals constructed by low-dimensional systems strengthens the light-matter interaction, leading to pronounced linear and nonlinear optical responses.[11] Moreover, the stacking diversity[10a] and possible ferroelectric polarization[12] of 1D building blocks in NLO crystals were expected to achieve tunable NLO applications. In addition, the predicted Te_7As_5I stacked with 1D Te_3As_2 and TeAsI chains demonstrates that NLO crystals stacked with 1D chains can obtain large SHG susceptibilities.[10a] The stacking of 1D chains makes it easy to break inversion symmetry, resulting in NLO crystals with large NLO coefficients and small bandgaps, which are in demand for infrared applications.

Starting from 3157 1D chains in the Computational 1D Materials Database (C1DB),[13] proper bandgaps, symmetry, the charge difference of the atoms on the chains (Δq), and stability are evaluated. We identified 21 1D chains with large SHG susceptibilities, which have static and peak SHG susceptibilities larger than 0.5% and 25% of the upper limit (two-band model), respectively. Fourteen of these chains are newly reported as NLO building blocks. Using these 21 chains from our high throughput screening (detailed information including their formula and properties are shown in **Table 1**) as building blocks, 45 new bulk vdW NLO crystals are constructed by considering lattice mismatch less than 5%. Among them, thirteen crystals contain only one kind of 1D chain, while the others contain two kinds of 1D chains. Eighteen of them inherit the large SHG susceptibilities of the

J. Yang, J. Pan, G. Wan, Y. Zhu, Z. Wei, Y. Li, S. Du
Beijing National Laboratory for Condensed Matter Physics and Institute of Physics
Chinese Academy of Sciences
Beijing 100190, China
E-mail: sxdu@iphy.ac.cn

J. Yang, J. Pan, Y.-F. Zhang, G. Wan, Y. Zhu, Z. Wei, Y. Li, S. Du
University of Chinese Academy of Sciences
Chinese Academy of Sciences
Beijing 100190, China

J. Pan, S. Du
Songshan Lake Materials Laboratory
Dongguan 523808, China

The ORCID identification number(s) for the author(s) of this article can be found under https://doi.org/10.1002/adfm.202411889

DOI: 10.1002/adfm.202411889

Table 1. Chemical formulas, sources, points groups, energy above convex hull (E_{hull}), charge differences of atoms on the chains (Δq), Gap types, HSE bandgaps (E_g), SHG peak locations (E_{peak}), SHG peak susceptibilities $\chi^{(2)}(0,0)$, static SHG susceptibilities $(\chi^{(2)}(0,0))$, and lattice constant along chain L for 21 1D NLO building blocks. For materials with several tensor elements in SHG susceptibilities, only the values of the highest are shown here. * represents unreported NLO building blocks.

Formula	Source	Point group	E_{hull} [eV per atom]	Δq	Gap type	HSE gap [eV]	E_{peak} [eV]	$\chi^{(2)}{}_{peak}$ [nm^3 V^{-1}]	$\chi^{(2)}(0,0)$ [nm^3 V^{-1}]	L [Å]
WBr_4O	Exp	C_4	0	2.939	Indirect	2.38	2.33	0.59	0.01	3.85
$NbBr_3O$	Exp	C_2	0	3.273	Indirect	3.10	3.77	0.47	0.012	3.91
WCl_4O	Exp	C_4	0	3.161	Indirect	3.36	2.33	0.37	0.0053	3.93
NbI_3O	Exp*	C_2	0	3.037	Direct	1.63	2.17	0.72	0.016	3.94
SO_3	Exp*	C_2	0	4.557	Direct	7.59	9.05	0.045	0.00046	4.15
PNF_2	Exp	C_2	0	5.756	Direct	7.75	4.64	0.051	0.00085	4.99
BPS_4	Exp	C_2	0	2.033	Indirect	3.54	4.38	0.13	0.0015	5.28
Be_2IBrCl_2	ML*	C_1	0.002	2.429	Direct	6.74	5.64	0.051	0.00042	5.46
$Ti_4Cl_4OS_9$	ES*	S_4	0	2.126	Indirect	2.57	2.64	0.46	0.02	5.56
$TaSbF_{10}$	ES*	C_1	0	3.559	Direct	7.16	5.74	0.045	0.00042	5.59
$Ti_4Br_4OS_9$	ES*	S_4	0	2.111	Indirect	2.37	2.61	0.47	0.027	5.59
$NbSbF_{10}$	Exp*	C_1	0	3.660	Direct	6.61	5.65	0.032	0.00049	5.62
$Ti_4I_4OS_9$	ES*	S_4	0	2.100	Indirect	1.96	2.91	0.46	0.046	5.63
$AlPS_4$	Exp	C_2	0	2.546	Indirect	4.14	5.09	0.11	0.00093	5.68
Be_2I_3Br	ML*	C_S	0.007	2.309	Indirect	5.92	3.65	0.063	0.0003	5.93
$TiZrBr_8$	ML*	C_1	0	2.360	Indirect	3.03	4.33	0.28	0.0034	6.43
$SnTi_5Br_{12}S_2$	ML*	C_1	0.004	2.009	Direct	1.31	1.74	3.48	0.064	7.13
Cr_2HgO_7	Exp*	C_1	0.010	2.340	Direct	3.70	3.86	0.066	0.0012	7.97
$I_2O_{11}S_2$	Exp*	C_1	0	3.976	Direct	4.07	2.47	0.13	0.0013	9.29
$LiSb_2F_7$	Exp*	C_2	0	2.299	Indirect	6.39	7.14	0.11	0.00039	9.69
$TeOF_2$	Exp	C_2	0	3.505	Direct	6.42	7.78	0.06	0.00049	11.44

corresponding 1D building blocks. Furthermore, we observed that the SHG susceptibilities, divided by their theoretical upper limit, exhibit a positive correlation with the electronic bandgaps. Additionally, the SHG susceptibilities are inversely proportional to the third power of the bandgaps, which differs from the upper limit of SHG susceptibility allowed by quantum mechanics (inversely proportional to the fourth power of bandgaps). Considering experimental synthesis and application, four new stable bulk crystals with large SHG susceptibilities or containing ferroelectric building blocks are obtained. By calculating the SHG spectrum of the experimentally synthesized 1D vdW NLO crystal $AlPS_4$, we found that the SHG susceptibility at 3.85 eV increases more than 300 times (or decreases to less than 1/300) when the stacking direction changes. The SHG spectrum of another experimentally synthesized 1D ferroelectric vdW NLO crystal $NbBr_3O$ shows that its SHG susceptibility changes as the ferroelectric polarization reversed, suggesting electric field tunable characteristics. Therefore, both the ferroelectric polarization and stacking order can be used to modulate nonlinear optic properties.

2. Results and Discussion

2.1. High Throughput Search of New 1D NLO Building Blocks

Figure 1a shows our workflow of screening NLO building blocks based on the 3157 1D chains in C1DB database, which are identified from experimentally synthesized bulk materials, element substitution, and machine learning. First, considering the computational complexity and potential of experimental realization and applications, nonmagnetic 1D chains with dynamic stability and energy above convex hull (E_{hull}) less than or equal to 10 meV per atom have been screened out. Detailed information including the source and criteria of E_{hull} are shown in Methods. Since suitable bandgaps are also required for the application of NLO crystals, 1D chains with a PBE bandgap larger than 0.4 eV are chosen, which are commonly used in NLO applications. Next, those 1D chains without inversion symmetry, which is required by SHG, are screened out for further processing. After removing the repetitive structures and crystals with radioactive elements, we relaxed these structures using first-principles calculations. By considering the bond links (Section 1, Experimental Section) and inversion symmetry after optimization, we obtained 51 1D NLO building blocks. The degree of the SHG susceptibilities approaches the frequency-dependent theoretical upper limit is of great significance for the design of NLO crystals. This is because the absorption edge is usually located near the bandgap, and the application scenarios of NLO crystals are influenced by the transparent region determined by the absorption edge. Once the application scenario is determined, achieving the maximum SHG output after meeting the bandgap requirements becomes the designer's goal. However, the resulting SHG susceptibilities vary due to differences in crystal symmetry, charge distribution, and other factors. The charge difference of the atoms on the chains (Δq) was found to be a useful descriptor for SHG susceptibility in the previous report.[10a] So, in order to find NLO 1D building blocks with SHG susceptibilities approaching theoretical upper

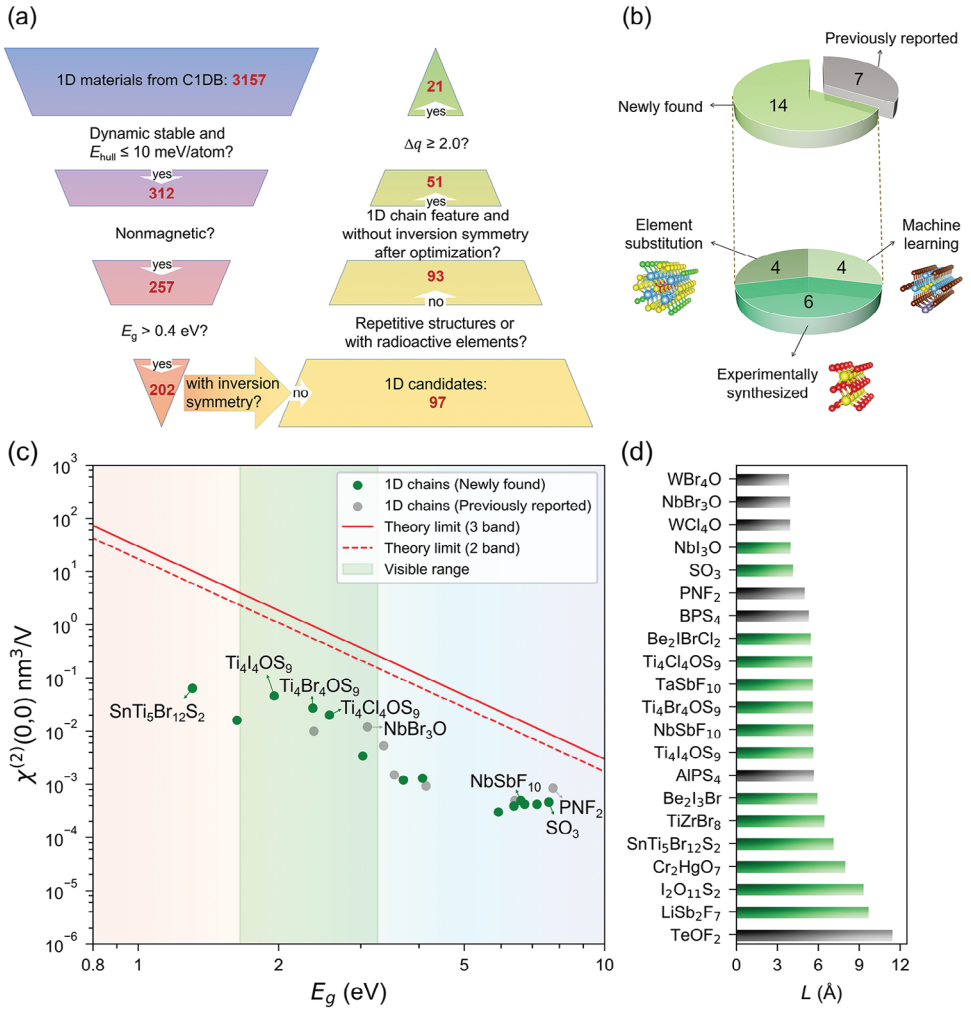

Figure 1. Screening process and the results of 1D building blocks for NLO crystals. a) Workflow for screening 1D NLO building blocks based on C1DB. E_{hull} is the energy above hull, and E_g is the electronic bandgaps. Δq is the average charge difference of neighboring atoms on the chain. b) Classification of 21 1D NLO building blocks including 14 newly reported. Among the 14 new building blocks, 6 of them are experimentally synthesized, while others are from either element substitution or machine learning. c) Static SHG susceptibilities ($\chi^{(2)}$(0,0)) as a function of bandgaps calculated by HSE06 functional for 1D NLO building blocks. Newly found NLO building blocks are marked as green dots, while previously reported are marked as grey ones. The red dashed line indicates the theoretical upper limit derived from the two-band model, while the red line indicates that derived from the three-band model. The visible light range is marked as a green patch. Only the largest element is shown here for crystals with several tensor elements of SHG susceptibilities. d) Lattice constants L along chains of 21 building blocks.

limit, chains with $\Delta q \geq 2.0$ are picked out as building blocks. This criteria of Δq is based on previously reported 1D vdW NLO crystals (Chapter 1, Supporting Information). Finally, we identified 21 1D NLO building blocks. As shown in Figure 1b, 14 of them have not been previously reported as NLO crystals. Among these 14 new 1D NLO building blocks, 6 are derived from experimentally synthesized bulk materials. Detailed information including formula, lattice constant, symmetry, $E_{hull,}$ and the charge difference of the atoms on the chains of these 1D NLO building blocks can be found in Table 1.

Next, the frequency-dependent linear optical dielectric functions and SHG susceptibilities of these newly found 1D NLO building blocks are calculated using the random phase approximation (RPA) (sum-over-states using independent electronic states).[14] As the Perdew-Burke-Ernzerhof (PBE) functional usually underestimates the bandgaps of semiconductors, a scissor correlation is adopted according to the bandgaps calculated with Heyd–Scuseria–Ernzerhof (HSE06) functional (Table 1). The detailed frequency-dependent linear optical dielectric functions, SHG susceptibilities, and crystal structures of these 1D materials can be found in Figures S2–S15 (Supporting Information). Figure 1c shows the static SHG susceptibilities ($\chi^{(2)}$(0,0)), the theoretical upper limits derived from the three band model (red line), and the two band model (red dashed line) of the screened-out 1D building blocks. Our results reveal that all the 1D NLO building blocks, including the newly found ones (green dots), have SHG susceptibilities close to the theoretical upper limits. The static and peak SHG susceptibilities of these building blocks are closer to the upper limits compared to 75% of bulk crystals composed of 1D building blocks in the previous report.[10a] Their

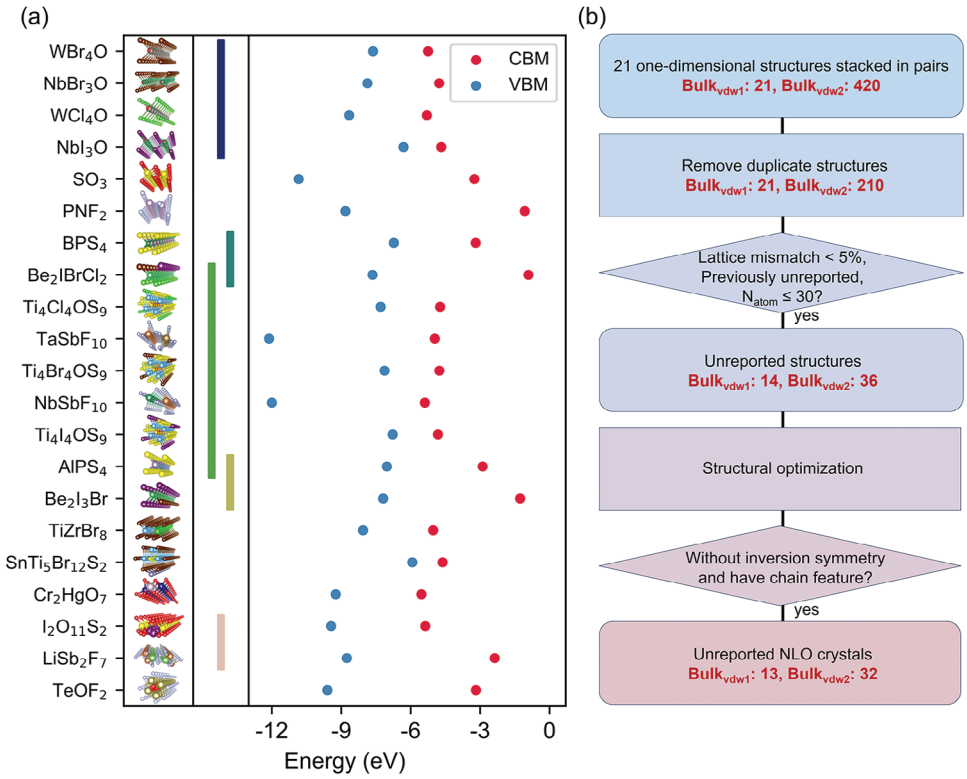

Figure 2. Selection and stacking of 1D building blocks. a) Formula, crystal structures, stacking feasibility, valence band maximum (VBM), and conduction band minimum (CBM) for 21 NLO building blocks. 1D building blocks with lattice mismatches smaller than 5% are considered stackable. Dark blue, light blue, green, yellow-green, and pink long stripes are used to mark the building blocks whose lattice mismatch is smaller than 5%. VBM and CBM are marked in blue and red dots, respectively. b) Workflow of constructing vdW NLO crystals from 1D NLO building blocks. N_{atom} is the number of atoms in the unit cell. By considering lattice matching, computational complexity, and removing duplicate crystals, crystals with inversion symmetry or without chain features, 13 bulk NLO crystals containing one kind of chain and 32 bulk NLO crystals containing two kinds of chains are finally obtained. $Bulk_{vdW1}$ and $Bulk_{vdW2}$ are crystals composed of 1 and 2 kinds of chains, respectively.

electronic bandgaps cover a wide spectrum from infrared, to visible and ultraviolet. Moreover, as shown in Figure S16 (Supporting Information), the 1D NLO building blocks with larger Δq tend to have larger bandgaps, static and peak SHG susceptibilities $\left(\chi^{(2)}_{peak}\right)$ closer to their theoretical upper limit. Peak SHG susceptibility is the highest value of SHG susceptibility shown in Figures S2–S15 (Supporting Information) which plot the SHG susceptibility as a function of excitation photon energy of the 14 1D materials. The lattice constants along chain direction for all calculated 1D materials (Figure 1d) range from 3 to 12 Å. The lattice constants determine the parameter settings for the theoretical upper limit (Section 2, Experimental Section). These building blocks can be used to construct crystals with good NLO properties.

2.2. Construction of NLO Bulk Materials with 1D Motifs

Considering the synthesis possibility and application, we then constructed 3D materials using the screened-out 1D building blocks. Compared to 2D building blocks, 1D building blocks exhibit more stacking prototypes. Here, we only considered AA stacking without any rotation from initial structures. The bandgap of a stacked crystal is one of the important factors that determine its NLO properties. In order to obtain NLO crystals with suitable absorption edges, the bandgaps of stacked crystals usually need to be larger than the working wave range. Due to the weak vdW interaction between chains, the bandgap of the stacked crystal can be predicted based on the 1D building blocks. First, we selected the 1D chains with suitable electronic bandgaps based on the desired working wave range. The bandgaps of the crystals stacked by one kind of chain should be similar to that of an isolated chain. In the case of crystals stacked by more than one kind of chain, the bandgaps should be related to the lowest conduction band minimum (CBM) and the highest valance band maximum (VBM) of all the building blocks.

$$E_g^{pre} = \min\left(E^i_{CBM}\right) - \max\left(E^i_{VBM}\right) \quad (1)$$

Where E_g^{pre} is the predicted bandgap of a stacked crystal. The $\min(E^i_{CBM})$ is the lowest energy of the CBMs, while the $\max(E^i_{VBM})$ is the highest energy of the VBMs of the isolated 1D building blocks, which have been calibrated by vacuum level.

The CBMs and VBMs of the 21 1D building blocks are shown in **Figure** 2a. The bandgaps cover infrared, visible, and ultraviolet ranges. We then constructed 3D crystals using the 21 1D building blocks (Figure 2b), generating 21 crystals composed of one kind

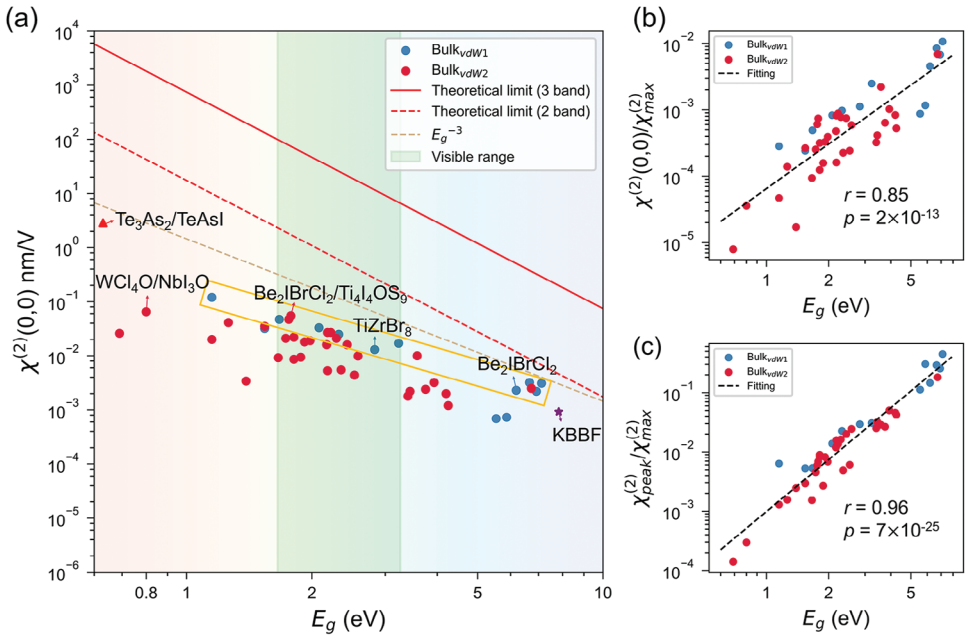

Figure 3. SHG susceptibilities, electronic bandgaps for 45 bulk vdW NLO crystals composed of 1D building blocks. a) Static SHG susceptibilities as a function of bandgaps for bulk vdW NLO crystals. Bulk vdW NLO crystals composed of one kind of building blocks (Bulk$_{vdw1}$) are marked in blue, while those composed of two kinds of building blocks (Bulk$_{vdw2}$) are marked in red. The SHG susceptibilities of the KBBF and Te_3As_2/TeAsI are also shown here for comparison. The red dashed line indicates the theoretical upper limit derived from the two band model, and the red line indicates the theoretical upper limit derived from the three-band model. The dark yellow dashed line indicates the E_g^{-3} relation. The visible-light range is marked as a green patch. Crystals with large SHG susceptibilities compared to other crystals in their wave range are marked with an orange rectangle. The largest element is shown for crystals with several tensor elements of SHG susceptibilities. b) Static SHG susceptibilities divided by theoretical upper limit (three band model) as a function of electronic bandgaps. c) Peak SHG susceptibilities divided by theoretical upper limit (three band model) as a function of electronic bandgaps. The black dashed lines are linear fitting of all the bulk vdW crystals composed of 1D building blocks. b) and c) both contain 45 samples. The value r is the Pearson correlation coefficient and the value p is from a two-sided test.

of chain and 210 crystals composed of two kinds of chains after removing duplicate structures. Here, we only considered chains with lattice mismatches smaller than 5% as building blocks. As shown in the middle panel of Figure 2a, dark blue, light blue, green, yellow-green, and pink long stripes are used to mark the building blocks whose lattice mismatch is smaller than 5%. In addition, for chains with small lattice constants, we created supercells to search for lattice-matching pairs (see Chapter 5, Supporting Information). Next, excluding previously reported crystals and crystals with more than 30 atoms, 14 bulk crystals composed of one kind of chain and 36 bulk crystals composed of two kinds of chains remain. Then, these structures are optimized using the first principles calculations. The bulk vdW crystals composed of 1D building blocks (judged by VESTA) without inversion symmetry after optimization are selected as new bulk vdW NLO crystals, including 13 bulk NLO crystals containing one kind of chains and 32 bulk NLO crystals containing two kinds of chains. Detailed information on constructing 3D crystals using 1D building blocks is presented in Chapter 8 of the Supporting Information. The calculated bulk bandgaps are consistent with the predicted bandgaps (Chapter 6, Supporting Information).

Figure 3a shows the static SHG susceptibilities and bandgaps calculated by HSE06 functional of the 45 newly constructed bulk vdW NLO crystals. The SHG susceptibilities of KBBF and Te_7As_5I are also shown here for comparison, as KBBF is a widely used deep ultraviolet NLO crystals with large SHG coefficients,[4a] while Te_7As_5I has the largest SHG susceptibility among all the predicted NLO crystals composed of 1D building blocks.[10a] Many of the newly constructed bulk vdW NLO crystals have SHG susceptibilities approaching the upper limit, similar to KBBF and Te_7As_5I. The theoretical upper limits derived from the two-band model and three-band model (Figure 3a) are inversely proportional to the fourth power of their bandgaps. So, we call it E_g^{-4} relations, which is the relation based on quantum mechanics.[15] Here, E_g is the energy bandgaps calculated using HSE06 functional. Interestingly, the largest SHG susceptibilities of the bulk vdW NLO crystals composed of 1D building blocks we obtained are proportional to E_g^{-3} (dark yellow dashed line in Figure 3a). This line is obtained by modifying the bandgap in the theoretical limit of the two band model from a quartic to a cubic relationship and multiplying by a constant, namely $|\chi^2(0,0)| \leq 5.2\times10^{17}\times\frac{24e^3}{\epsilon_0}\frac{{E_0}^2\Xi}{E_g^3}$. It effectively reflects the distribution of maximum SHG susceptibilities. As shown in Figure 3b,c, $\chi^{(2)}(0,0)/\chi^{(2)}_{max}$ and $\chi^{(2)}_{peak}/\chi^{(2)}_{max}$ are positively correlated with the electronic bandgaps. The $\chi^{(2)}_{max}$ is the theoretical upper limit of SHG susceptibilities derived from three-band model. After applying logarithm transformation, we calculated the Pearson linear correlation coefficient and found $r = 0.85$ for $\chi^{(2)}(0,0)/\chi^{(2)}_{max}$, and $r = 0.96$ for $\chi^{(2)}_{peak}/\chi^{(2)}_{max}$. These correlations are highly significant as $p = 2\times10^{-13} < 0.001$ for $\chi^{(2)}(0,0)/\chi^{(2)}_{max}$ and

$p = 7 \times 10^{-25} < 0.001$ for $\chi^{(2)}_{peak}/\chi^{(2)}_{max}$. The Pearson correlation coefficient r is the ratio between the covariance of two variables and the product of their standard deviations, reflecting linear correlation of two datasets. While p is the probability under the null hypothesis of obtaining a real-valued test statistic at least as extreme as the one obtained, indicating the significance of correlation of two datasets. For bulk crystals composed of 1D chains, a larger Δq does make them easier to approach the theoretical upper limit, but a larger Δq can also result in a larger bandgap (Figure S16, Supporting Information). Although the SHG susceptibilities of crystals with wider bandgaps will be closer to the theoretical upper limit, NLO crystals with narrower bandgaps can have larger SHG susceptibility due to higher upper limit and can be used in applications working at longer wavelengths. In the following discussion, we tend to compare the SHG susceptibilities of NLO crystals with similar bandgaps.

Among the 45 newly constructed vdW NLO crystals, 18 of them exhibit large static SHG susceptibilities compared to the crystals with similar bandgaps and are marked in orange rectangles in Figure 3a. Considering the experimental synthesis and application prospects, their dynamic and thermodynamic stabilities are evaluated by first-principles calculations. Be_2IBrCl_2, $TiZrBr_8$, $Be_2IBrCl_2/Ti_4I_4OS_9$ emerge as stable NLO crystals (Chapter 7, Supporting Information) with large SHG susceptibilities and birefringence (Chapter 8, Supporting Information). In addition, the stabilities of crystals containing ferroelectric 1D building blocks are also evaluated, which may bring applications in tunable nonlinear optics and NLO switches. WCl_4O/NbI_3O is found to be dynamically and thermodynamically stable. (Figure S21, Supporting Information).

2.3. Potential Applications of Tunable SHG Susceptibilities in NLO Crystals

Stacking order[6,16] and ferroelectric polarization[17] were reported to modulate NLO properties. Both strategies are applicable in bulk crystals composed of 1D building blocks. Taking experimentally synthesized crystals composed of 1D building blocks as an example, we demonstrated the effects of such transitions on NLO properties.

As an experimentally synthesized crystal composed of 1D building blocks, bulk $AlPS_4$[18] has two phases. Lt-$AlPS_4$ ($P\bar{4}2c$) consists of 1D building blocks stacked along different orientations in neighboring layers, while ht-$AlPS_4$ ($I222$) consists of 1D building blocks stacked along the same direction (**Figure 4a**). The phase transition from lt-$AlPS_4$ to ht-$AlPS_4$ has been realized in experiment by heating.[18] However, the impact of this phase transition on nonlinear optics has not been previously studied. Our calculations on the frequency-dependent SHG susceptibilities of the two phases reveal that the staking orientation brings significant changes to the SHG susceptibilities (Figure 4b,c). As phase transition happens from lt-$AlPS_4$ to ht-$AlPS_4$, the static SHG susceptibilities of $\chi^{(2)}_{xyz}$ and $\chi^{(2)}_{zxy}$ change from 0.01 to 0.002 nm V^{-1}, while the SHG susceptibilities at 3.85 eV of $\chi^{(2)}_{zxy}$ changes significantly from 0.126 to 0.0004 nm V^{-1}. According to Bader analysis, we found that the charge differences of the atoms on the chains (Δq) in lt-$AlPS_4$ and ht-$AlPS_4$ are almost identical, with 2.55 e and 2.56 e respectively. Previous studies have shown that the density of states (DOS) at the band edge plays a crucial role in NLO coefficients.[19] A higher DOS at the band edge implies a higher two-photon absorption probability,[20] leading to larger SHG susceptibilities.[11,21] The calculated DOS at the band edge shows a noticeable change (Figure S27a–d, Supporting Information). The valence band edge is mainly contributed by the p orbitals of S, while the conduction band edge is contributed by the p orbitals of S and s orbital of P (Figure S27b,d, Supporting Information). The stacking configuration difference makes the electron density at conduction band edge of ht-$AlPS_4$ much lower than that of lt-$AlPS_4$. As shown in Figure S27a,c (Supporting Information), the first DOS peak near the conduction band edge of ht-$AlPS_4$ is positioned at a far energy state from the band edge and exhibits a smaller height relative to lt-$AlPS_4$.

Thus, the significant SHG susceptibilities difference between lt-$AlPS_4$ and ht-$AlPS_4$ is due to the change in stacking configuration, leading to the change in vdW interaction and electronic structures, particularly the DOS at band edges. Considering that the calculation of the DOS is less computationally expensive than that of SHG susceptibilities, the DOS at band edges can be used as a criterion to look for suitable stacking configurations when designing vdW NLO crystals. This approach is expected to accelerate the design and discovery of vdW NLO crystals.

The ferroelectric transition has been reported to realize reversible variation of SHG intensity.[17] $NbBr_3O$ is an experimentally synthesized bulk material[22] composed of ferroelectric 1D building blocks. It has stable ferroelectric state FE, antiferroelectric states AFE-1 and AFE-2[12a] (**Figure 5a–c**). The SHG susceptibilities of $NbBr_3O$ at different polarization states are calculated to investigate the effect of ferroelectric polarization on NLO properties. As shown in Figure 5d,e, the variation of ferroelectric polarization brings significant changes to the SHG susceptibilities. Due to different symmetries of AFE-1 and FE states, their non-zero SHG components are completely different (Figure 5 d,e). Moreover, all the SHG components of AFE-2 state reduce to zero due to its inversion symmetry (Figure 5f). Interestingly, for ferroelectric NLO crystal $NbBr_3O$, the magnitudes of SHG susceptibilities are closely related to the polarization directions of ferroelectric chains. The SHG susceptibility is enhanced when the polarizations are in the same directions (FE state, Figure 5d), while it is weakened when the polarizations are in the opposite directions (AFE state, Figure 5e,f). Because the SHG process is related to the dipole-like charge distribution, it is reflected by the charge difference of the atoms on the chain for 1D chain.[10a] For crystals composed of 1D chains, the micro SHG responses of the chains will accumulate if each chain exhibits the same polarization directions, while they will compensate if neighboring chains exhibit opposite polarization directions. This is also the reason why the SHG susceptibilities of crystals with inversion symmetry are zero. More importantly, ferroelectric polarization reversal of $NbBr_3O$ has been predicted to be easily realized in experiments with a small energy barrier.[23] Therefore, the modulation of SHG susceptibilities by tuning ferroelectric polarization makes $NbBr_3O$ a good candidate to realize NLO switching. Such a process brings attractive optoelectronic and photonic application prospects, including signal processing, sensors, broad-spectral optical frequency converters, etc.[24]

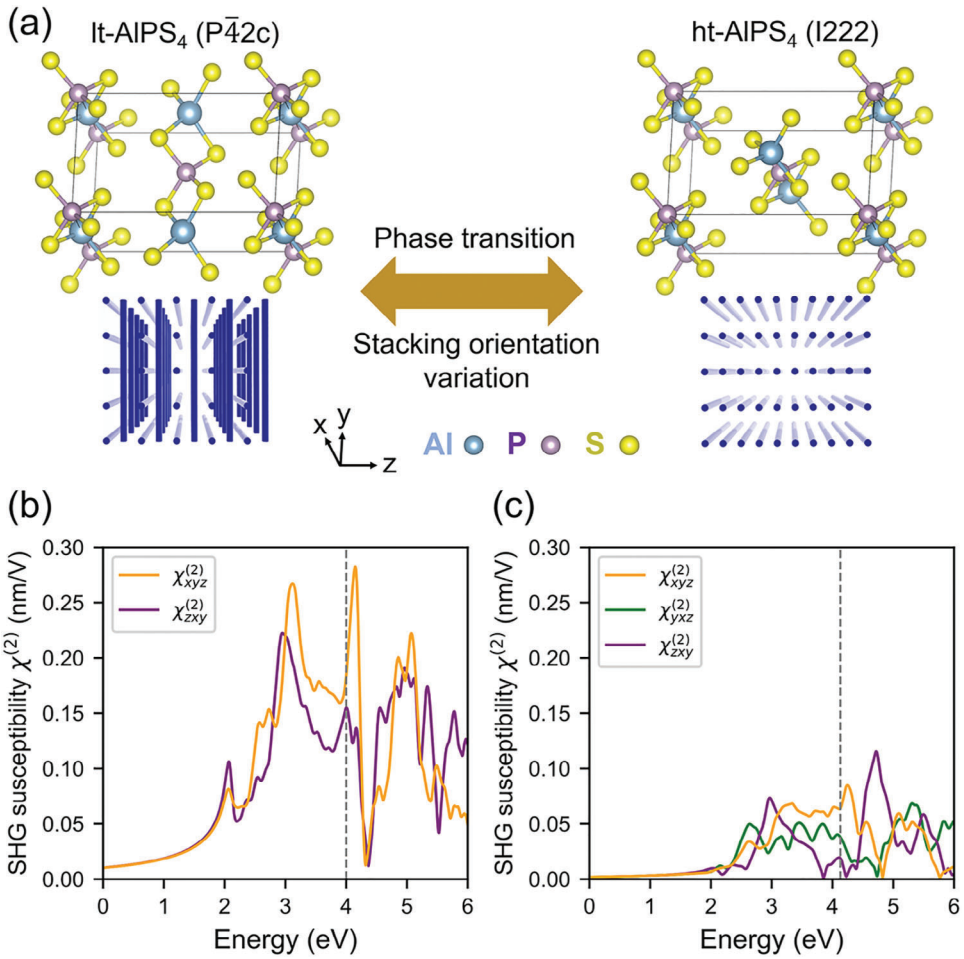

Figure 4. Stacking orientation-related SHG susceptibilities of $AlPS_4$. a) Crystal structures and schematics of lt-$AlPS_4$ (P $\bar{4}$ 2c) and ht-$AlPS_4$ (I222). b,c) Frequency-dependent SHG susceptibilities of lt-$AlPS_4$ (P $\bar{4}$ 2c) and ht-$AlPS_4$ (I222), respectively. Absorption edges are marked with grey dotted lines.

3. Conclusion

In conclusion, we have identified 21 1D NLO building blocks with large SHG susceptibilities through high-throughput calculations. Among them, 14 are newly identified as NLO building blocks. By stacking one or two kinds of 1D building blocks, we obtained 13 bulk crystals composed of one kind of 1D building blocks and 32 bulk crystals composed of two kinds of 1D building blocks. Their SHG susceptibilities vary more smoothly with the bandgap ($\propto E_g^{-3}$) compared to the upper limit of SHG susceptibilities allowed by quantum mechanics ($\propto E_g^{-4}$). Considering experimental synthesis and application potential, the stabilities of the bulk crystals with large SHG susceptibilities or containing ferroelectric building blocks are evaluated. Be_2IBrCl_2, $TiZrBr_8$, $Be_2IBrCl_2/Ti_4I_4OS_9$, and WCl_4O/NbI_3O emerge as stable bulk NLO crystals with promising application potential. In addition, based on two experimentally synthesized bulk crystals composed of 1D building blocks, we demonstrated that the temperature-driven phase transition of $AlPS_4$ between the vertical and parallel stacking directions can bring significant changes in their SHG susceptibilities. Moreover, the conversion between different ferroelectric states of $NbBr_3O$ can modulate the SHG susceptibilities, suggesting the potential application in NLO switching.

Finally, we provide an outlook on the synthesis of these vdW crystals composed of 1D chains. Unlike traditional 1D vdW heterostructures,[25] the vdW crystals mentioned here are all bulk crystals with both thermodynamic and dynamic stability. Like molecular crystals, they can crystallize directly through physical or chemical methods. There were related synthesis cases as early as the last century. For example, Te_7As_5I is a vdW crystal composed of two different chains, which has been successfully prepared as a byproduct at high temperatures. The key to synthesis lies in suitable temperatures and reactant ratios.[26] Another example of heterogeneous vdW crystals is the $(MX_4)_nY$ class of compounds, which can similarly be obtained by simply heating elemental substances.[27] Although large single crystals required for NLO applications have higher synthesis difficulties, the excellent properties of vdW crystals composed of 1D chains are worth further exploration. We hope to rekindle interest in the synthesis of vdW crystals composed of 1D chains. Their significance extends beyond NLO applications and brings unique electrical, thermal, and topological properties.[28]

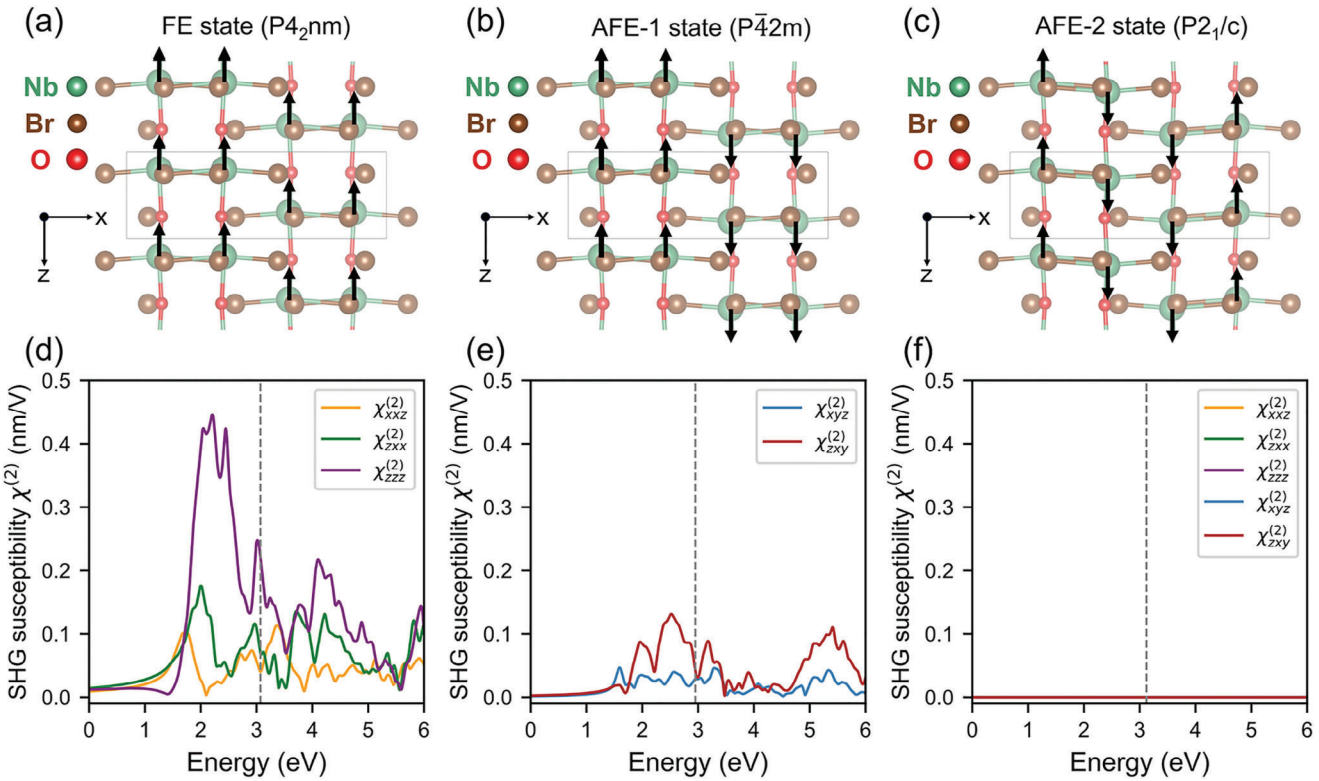

Figure 5. The structures and SHG susceptibilities of $NbBr_3O$ at different ferroelectric polarization states. a–c) Crystal structures of $NbBr_3O$ at FE, AFE-1, and AFE-2 states. The black arrows represent the polarization that comes from the upward or downward displacement of Nb atoms. d–f) Frequency-dependent SHG susceptibilities of $NbBr_3O$ at FE, AFE-1, and AFE-2 states, respectively. Absorption edges are marked with grey dotted lines.

4. Experimental Section

DFT Calculation: Geometric relaxations and charge distribution of NLO materials were calculated using density functional theory (DFT) within projector-augmented wave (PAW) potentials and the Perdew-Burke-Ernzerhof (PBE) exchange-correlation functional[29] as implemented in the Vienna ab initio simulation package (VASP) code. Bader analysis[30] was then used to calculate the charge difference of atoms on the chain (Chapter 1, Supporting Information). Due to the computational costs, we used PBE bandgap in screening process. After screening, energy bandgap and vacuum level were calculated using VASP with the Heyd–Scuseria–Ernzerhof exchange-correlation 06 (HSE06) functional.[31] Dynamic stability was demonstrated by phonon spectral calculations based on finite differences (FD), density functional perturbation theory (DFPT), and PHONOPY.[32] A plane-wave basis set with an energy cutoff of 550 eV was used, and the vdW-dispersion energy-correction term was considered by the DFT-D3 method,[33] which was derived by Grimme et al. Monkhorst–Pack[34] Brillouin zone sampling grids with a resolution of $0.02 \times 2\pi$ Å^{-1} were applied. The structures studied here were fully relaxed until force was converged to 0.01 eV Å^{-1}. The 1D building blocks were repeated periodically in supercells, including a 20 Å vacuum between chains. A variant of the cell index method[35] was adopted by VESTA[36] to identify the bonds. A key factor indicating the thermodynamic stability of a compound was its heat of formation (ΔH). For a binary compound with the composition A_nB_m, the heat of formation per atom was defined as $\Delta H = \frac{E(A_nB_m) - nE(A) - mE(B)}{n+m}$, where $E(A_nB_m)$ represents the total energy per unit cell of the compound, and $E(A)$, $E(B)$ are the energies per atom in the standard states of elements A and B, respectively. This definition can be extended to compounds containing more than two elements. A large heat of formation suggests that the compound is likely to decompose into its constituent elements, while a small or negative value indicates its thermodynamic stability. This concept can also be applied to the decomposition of a compound into other materials, not just elements, which is explored through convex hull construction.[37] For specific compositions such as $A_nB_mC_p$, the combination of materials with that composition and the lowest heat of formation will lie on the convex hull. The energy of a material relative to this convex hull is denoted as E_{hull}. For thermodynamic stability of 1D chains, the E_{hull} values from the C1DB database were used.[13] They used all relevant elemental, binary, and ternary compounds including bulk crystals that reside on the convex hull in the OQMD database.[38] The structures and energies were recalculated using the GPAW method with the PBE-D3 functional. Considering the high thermal stability requirements for NLO applications, $\leq$10 meV per atom was selected as the threshold. An E_{hull} value larger than 10 meV per atom does not imply the synthesis was impossible. However, this criterion was beneficial for obtaining highly stable crystals. For crystals formed by one kind of chain in the work, their E_{hull} was lower than that of the single chains, indicating that they are stable. For crystals composed of two kinds of chains, obtaining the convex hull is quite complex due to the greater number of elements. Therefore, as an alternative, 300 K Ab Initio Molecular Dynamics (AIMD) simulations were used to assess their thermodynamic stability at room temperature.

The frequency-dependent linear optical dielectric function, second-order nonlinear optical susceptibility, absorption spectrum, and refractive index spectrum were calculated by the first principles simulation package ABINIT[39] with RPA approximation.[14] We adopted the generalized gradient approximation (GGA) in the form of the PBE for the exchange-correlation potentials. The PAW pseudopotentials were used with a plane wave energy of 50 Hartree. a Monkhorst–Pack k-point set with a resolution of $0.015 \times 2\pi$ Å^{-1} was used to sample the Brillouin zone. The number of empty bands was set to be three times that of the occupied states. Through

the band gap value calculated by the HSE06 functional, the scissor correction was applied to a frequency-dependent linear optical dielectric function, second-order nonlinear optical susceptibility, absorption spectrum, and refractive index spectrum. The calculated second-order nonlinear coefficients by this method were tested to be consistent with those in other references.[40]

Theoretical Upper Limit: The upper limit of NLO responses originates from the fact that transition dipole matrix elements in quantum systems cannot be infinity. The equations of upper limits for the SHG susceptibility allowed by quantum mechanics are:

$$\left|\chi^2\ (0,0)\right| \leq \frac{24e^3}{\varepsilon_0}\frac{{E_0}^2\Xi}{E_g^4} \tag{2}$$

$$\left|\chi^2\ (0,0)\right| \leq \frac{3e^3\hbar^3}{\varepsilon_0 m^2 V_{uc}}\frac{P_0}{E_g^4} \tag{3}$$

The models here are nonmagnetic cold semiconductor systems without spin-orbit coupling in long-wavelength limit and dipole approximation. Both equations focus on the diagonal element of the susceptibility tensor. According to the number of energy bands considered, models are divided into two-band models and three-band models. Equation (2) was derived from the two-band model with one conduction band and one valence band.[15] Here, e and m are the charge and mass of the electron, while Ξ denotes a dimensionless quantity. E_0 is energy that depends only weakly on the bandgap, and E_g is the electronic bandgap. The values of $\Xi = 1$, $E_0 = 0.2$ eV are adopted. Meanwhile, Equation (3) was derived from the three-band model with one valence and two conduction bands.[40] Here, P_0 is the maximum magnitude of the momentum matrix element, and the value of $P_0 = \hbar/a_B$ is used, where a_B is Bohr radius. V_{uc} is the unit cell volume for bulk materials. Well-defined 1D SHG susceptibilities can be obtained by replacing V_{uc} with the unit cell length (L_{uc}) for 1D building blocks in Equation (3) and calculation of SHG susceptibilities. Derived lattice constants L are defined as $\sqrt[3]{V_{uc}}$ for 3D crystals. A derived lattice constant of 2 Å (near the smallest lattice constant of our crystals) is used in the three-band model here.

Statistical Analysis: Due to the large differences (several orders of magnitude) in the SHG susceptibilities of NLO crystals with varying bandgaps and Δq, the data in Figure 3b,c was presented using logarithmic coordinates. These figures include 45 samples, namely, 45 bulk crystals constructed from 1D building blocks. The correlation and significance were described using the Pearson correlation coefficient r and the two-sided p-value from hypothesis testing. The statistical software that was used comes from the "Stats" module of the SciPy package run by Python.

Supporting Information

Supporting Information is available from the Wiley Online Library or from the author.

Acknowledgements

This work was supported by funds from the National Key Research and Development Program of China (2022YFA1204100, 2021YFA1201501), the National Natural Science Foundation of China (62488201, 52272172), the Major Program of the National Natural Science Foundation of China (92163206), and the Fundamental Research Funds for the Central Universities. Computational resources were provided by the Tier 3 Data Center in Ulanqab and National Supercomputing Center in Tianjin.

Conflict of Interest

The authors declare no conflict of interest.

Author Contributions

S.D. conceived and supervised the research project. J.Y. performed the first principles calculations and data analysis. J.Y. wrote the manuscript. All authors participated in discussing and editing the manuscripts.

Data Availability Statement

The data that support the findings of this study are available on request from the corresponding author. The data are not publicly available due to privacy or ethical restrictions.

Keywords

1D building blocks, nonlinear optics, second harmonic generation, semiconductors, tunable nonlinear optics

Received: July 5, 2024
Revised: October 9, 2024
Published online: November 19, 2024

[1] a) I. Cristiani, V. Degiorgio, *Riv. Nuovo Cimento* **2004**, *27*, 1; b) P. A. Franken, G. Weinreich, C. W. Peters, A. E. Hill, *Phys. Rev. Lett.* **1961**, *7*, 118.
[2] a) R.-M. Ma, R. F. Oulton, V. J. Sorger, X. Zhang, *Laser Photonics Rev.* **2013**, *7*, 1; b) L. Liu, D. S. Lu, W. B. Chen, T. Li, Q. Z. Qu, B. Wang, L. Li, W. Ren, Z. R. Dong, J. B. Zhao, W. B. Xia, X. Zhao, J. W. Ji, M. F. Ye, Y. G. Sun, Y. Y. Yao, D. Song, Z. G. Liang, S. J. Hu, D. H. Yu, X. Hou, W. Shi, H. G. Zang, J. F. Xiang, X. K. Peng, Y. Z. Wang, *Nat. Commun.* **2018**, *9*, 2760.
[3] a) W. B. Cai, A. Abudurusuli, C. W. Xie, E. Tikhonov, J. J. Li, S. L. Pan, Z. H. Yang, *Adv. Funct. Mater.* **2022**, *32*, 2200231; b) M. Mutailipu, S. Pan, *Angew. Chem., Int. Ed.* **2020**, *59*, 20302.
[4] a) B. C. Wu, D. Y. Tang, N. Ye, C. T. Chen, *Opt. Mater.* **1996**, *5*, 105; b) X. Zhao, C. Lin, C. Wang, H. Tian, T. Yan, B. Li, N. Ye, M. Luo, *Angew. Chem., Int. Ed.* **2024**, *63*, 202319424; c) B. Lu, S. Sayyad, M. Á. Sánchez-Martínez, K. Manna, C. Felser, A. G. Grushin, D. H. Torchinsky, *Phys. Rev. Res.* **2022**, *4*, L022022; d) V. K. Gudelli, G.-Y. Guo, *New J. Phys.* **2021**, *23*, 093028; e) S. Patankar, L. Wu, B. Lu, M. Rai, J. D. Tran, T. Morimoto, D. E. Parker, A. G. Grushin, N. L. Nair, J. G. Analytis, J. E. Moore, J. Orenstein, D. H. Torchinsky, *Phys. Rev. B* **2018**, *98*, 165113.
[5] a) J. Shi, S. Feng, P. He, Y. Fu, X. Zhang, *Molecules* **2023**, *28*, 6737; b) S. J. Brun, T. G. Pedersen, *Phys. Rev. B* **2015**, *91*, 205405; c) P. Yang, W. Feng, G.-B. Liu, G.-Y. Guo, Y. Yao, *Phys. Rev. B* **2023**, *107*, 214437.
[6] Q. Wu, L. Kang, J. Wu, Z. Lin, *npj Comput. Mater.* **2023**, *9*, 171.
[7] G. Ting, P. X. Qiu, F. C. Lin, *Nonlinear Opt.* **1991**, *1409*, 24.
[8] S. Nath, A. Puthukkudi, J. Mohapatra, B. P. Biswal, *Angew. Chem., Int. Ed.* **2023**, *62*, 202218974.
[9] a) L. Kang, P. Gong, Z. Lin, B. Huang, *Angew. Chem., Int. Ed.* **2021**, *60*, 16680; b) Y. Liu, X. Liu, Z. Xiong, B. Liu, J. Xu, L. Li, S. Zhao, Z. Lin, M. Hong, J. Luo, *Inorg. Chem.* **2021**, *60*, 14544.
[10] a) J. Yang, J. Deng, J. Pan, Y. Zhu, Y. F. Zhang, Y. Li, J. T. Sun, S. Du, *Adv. Funct. Mater.* **2023**, *33*, 2305731; b) L. Kang, X. Zhang, F. Liang, Z. Lin, B. Huang, *Angew. Chem., Int. Ed.* **2019**, *58*, 10250; c) M. Cheng, S. Wu, Z.-Z. Zhu, G.-Y. Guo, *Phys. Rev. B* **2019**, *100*, 035202.
[11] G. Wang, S. Mei, J. Liao, W. Wang, Y. Tang, Q. Zhang, Z. Tang, B. Wu, G. Xing, *Small* **2021**, *17*, 2100809.
[12] a) W. Sun, N. Ding, J. Chen, H.-P. You, J. Peng, S.-S. Wang, S. Dong, *Phys. Rev. Mater.* **2022**, *6*, 104404; b) L. T. Ye, W. J. Zhou, D. J. Huang, X. Jiang, Q. B. Guo, X. Y. Cao, S. H. Yan, X. Y. Wang, D. H. Jia, D. Q.

Jiang, Y. G. Wang, X. Q. Wu, X. Zhang, Y. Li, H. C. Lei, H. Y. Gou, B. Huang, *Nat. Commun.* **2023**, *14*, 5911.
[13] H. Moustafa, P. M. Larsen, M. N. Gjerding, J. J. Mortensen, K. S. Thygesen, K. W. Jacobsen, *Phys. Rev. Mater.* **2022**, *6*, 064202.
[14] S. Sharma, C. Ambrosch-Draxl, *Phys. Scr.* **2004**, *T109*, 128.
[15] L. Z. Tan, A. M. Rappe, *Phys. Rev. B* **2019**, *100*, 085102.
[16] Q. Wu, F. Liang, L. Kang, J. Wu, Z. Lin, *ACS Appl. Mater. Interfaces* **2022**, *14*, 9535.
[17] Y. Song, H. Yu, B. Li, X. Li, Y. Zhou, Y. Li, C. He, G. Zhang, J. Luo, S. Zhao, *Adv. Funct. Mater.* **2023**, *34*, 2310407.
[18] A. Kuhn, R. Eger, P. Ganter, V. Duppel, J. Nuss, B. V. Lotsch, *Z. Anorg. Allg. Chem.* **2014**, *640*, 2663.
[19] a) Q. Wu, C. Yang, X. Liu, J. Ma, F. Liang, Y. Du, *Mater. Today Phys.* **2021**, *21*, 100569; b) J. Xu, X. Li, J. Xiong, C. Yuan, S. Semin, T. Rasing, X. H. Bu, *Adv. Mater.* **2020**, *32*, 1806736.
[20] W. Chen, F. Zhang, C. Wang, M. Jia, X. Zhao, Z. Liu, Y. Ge, Y. Zhang, H. Zhang, *Adv. Mater.* **2021**, *33*, 2004446.
[21] X. F. Liu, Q. B. Guo, J. R. Qiu, *Adv. Mater.* **2017**, *29*, 1605886.
[22] S. Hartwig, H. Hillebrecht, *Z. Anorg. Allg. Chem.* **2007**, *634*, 115.
[23] L. Zhang, C. Tang, S. Sanvito, A. Du, *npj Comput. Mater.* **2021**, *7*, 135.
[24] a) Y. Q. Shi, C. Zhang, H. Zhang, J. H. Bechtel, L. R. Dalton, B. H. Robinson, W. H. Steier, *Science* **2000**, *288*, 119; b) K. A. Green, M. P. Cifuentes, T. C. Corkery, M. Samoc, M. G. Humphrey, *Angew. Chem., Int. Ed.* **2009**, *48*, 7867; c) P. C. Ray, *Chem. Rev.* **2010**, *110*, 5332; d) T. Y. Ma, N. N. Ma, L. K. Yan, T. Zhang, Z. M. Su, *J. Phys. Chem. A* **2013**, *117*, 10783; e) W. F. Chen, B. W. Liu, S. M. Pei, Q. N. Yan, X. M. Jiang, G. C. Guo, *Chem. Mater.* **2021**, *33*, 3729; f) K. K. Han, X. Ye, B. Li, Z. H. Wei, J. Wei, P. Wang, H. Cai, *Inorg. Chem.* **2022**, *61*, 11859; g) P. Wang, M. X. Zhang, Z. H. Wei, W. Q. Du, Z. Q. Peng, H. Cai, *Inorg. Chem.* **2022**, *61*, 16414; h) Y.-C. Yang, X. Liu, X.-B. Deng, L.-M. Wu, L. Chen, *JACS Au* **2022**, *2*, 2059.
[25] J. Guo, R. Xiang, T. Cheng, S. Maruyama, Y. Li, *ACS Nanosci. Au* **2022**, *2*, 3.
[26] R. Kniep, H. D. Reski, *Zeitschrift für Naturforschung B* **1982**, *37b*, 151.
[27] P. Gressier, A. Meerschaut, L. Guemas, J. Rouxel, P. Monceau, *J. Solid State Chem.* **1984**, *51*, 141.
[28] A. A. Balandin, F. Kargar, T. T. Salguero, R. K. Lake, *Mater. Today* **2022**, *55*, 74.
[29] J. Paier, R. Hirschl, M. Marsman, G. Kresse, *J. Chem. Phys.* **2005**, *122*, 234102.
[30] a) G. Henkelman, A. Arnaldsson, H. Jonsson, *Comput. Mater. Sci.* **2006**, *36*, 354; b) E. Sanville, S. D. Kenny, R. Smith, G. Henkelman, *J. Comput. Chem.* **2007**, *28*, 899; c) W. Tang, E. Sanville, G. Henkelman, *J. Phys.:Condes. Matter* **2009**, *21*, 084204; d) M. Yu, D. R. Trinkle, *J. Chem. Phys.* **2011**, *134*, 064111.
[31] a) J. Heyd, G. E. Scuseria, M. Ernzerhof, *J. Chem. Phys.* **2003**, *118*, 8207; b) A. V. Krukau, O. A. Vydrov, A. F. Izmaylov, G. E. Scuseria, *J. Chem. Phys.* **2006**, *125*, 224106.
[32] A. Togo, I. Tanaka, *Scr. Mater.* **2015**, *108*, 1.
[33] a) S. Grimme, J. Antony, S. Ehrlich, H. Krieg, *J. Chem. Phys.* **2010**, *132*, 154104; b) R. Car, M. Parrinello, *Phys. Rev. Lett.* **1985**, *55*, 2471.
[34] H. J. Monkhorst, J. D. Pack, *Phys. Rev. B* **1976**, *13*, 5188.
[35] B. Quentrec, C. Brot, *J. Comput. Phys.* **1973**, *13*, 430.
[36] K. Momma, F. Izumi, *J. Appl. Crystallogr.* **2011**, *44*, 1272.
[37] a) C. B. Barber, D. P. Dobkin, H. Huhdanpaa, *ACM Trans. Math. Software* **1996**, *22*, 469; b) A. R. Akbarzadeh, V. Ozoliņš, C. Wolverton, *Adv. Mater.* **2007**, *19*, 3233.
[38] S. Kirklin, J. E. Saal, B. Meredig, A. Thompson, J. W. Doak, M. Aykol, S. Rühl, C. Wolverton, *npj Comput. Mater.* **2015**, *1*, 15010.
[39] a) X. Gonze, J. M. Beuken, R. Caracas, F. Detraux, M. Fuchs, G. M. Rignanese, L. Sindic, M. Verstraete, G. Zerah, F. Jollet, M. Torrent, A. Roy, M. Mikami, P. Ghosez, J. Y. Raty, D. C. Allan, *Comput. Mater. Sci.* **2002**, *25*, 478; b) X. Gonze, B. Amadon, P. M. Anglade, J. M. Beuken, F. Bottin, P. Boulanger, F. Bruneval, D. Caliste, R. Caracas, M. Cote, T. Deutsch, L. Genovese, P. Ghosez, M. Giantomassi, S. Goedecker, D. R. Hamann, P. Hermet, F. Jollet, G. Jomard, S. Leroux, M. Mancini, S. Mazevet, M. J. T. Oliveira, G. Onida, Y. Pouillon, T. Rangel, G. M. Rignanese, D. Sangalli, R. Shaltaf, M. Torrent, et al., *Comput. Phys. Commun.* **2009**, *180*, 2582; c) X. Gonze, F. Jollet, F. A. Araujo, D. Adams, B. Amadon, T. Applencourt, C. Audouze, J. M. Beuken, J. Bieder, A. Bokhanchuk, E. Bousquet, F. Bruneval, D. Caliste, M. Cote, F. Dahm, F. Da Pieve, M. Delaveau, M. Di Gennaro, B. Dorado, C. Espejo, G. Geneste, L. Genovese, A. Gerossier, M. Giantomassi, Y. Gillet, D. R. Hamann, L. He, G. Jomard, J. L. Janssen, S. Le Roux, et al., *Comput. Phys. Commun.* **2016**, *205*, 106.
[40] A. Taghizadeh, K. S. Thygesen, T. G. Pedersen, *ACS Nano* **2021**, *15*, 7155.